RSC Applied Interfaces

ROYAL SOCIETY OF CHEMISTRY

PAPER

View Article Online
View Journal | View Issue

Cite this: *RSC Appl. Interfaces*, 2024, **1**, 173

Highly efficient oil-fouling and foam removal achieved by surfactant mixed systems†

Zeyu Zhao,[ad] Tengda Wang,[bc] Jiling Yue,[a] Yaxun Fan *[abc] and Yilin Wang *[abcd]

Excessive usage of surfactants in daily life and industry and their undesirable high foamability have caused serious environmental pollution and economic loss. Improving cleaning efficiency and reducing foam stability concurrently is a delicate strategy but a challenging task. Herein, we mixed the most widely used surfactant sodium dodecyl sulfate (SDS) with cyclic amines (C_nN, n = 6, 8, 12), by which the self-assembly ability of SDS at the air/water interface and in bulk is significantly enhanced, while spherical micelles, vesicles and wormlike micelles are formed at appropriate total surfactant concentration (C_T) and molar fraction of SDS (X_{SDS}). Especially around X_{SDS} = 0.50 and above critical micellar concentration (CMC), the stronger self-assembly ability leads to a higher contact angle of machine oil on stainless-steel plates and lower oil–water interfacial tension in C_nN/SDS solution, thus the oil-fouling removal efficiency of C_nN/SDS solutions is remarkably improved. Meanwhile, the foamability and foam stability dramatically decline at smaller X_{SDS} and slightly above CMC, attributed to the rapid molecular migration from liquid film of foams to the bulk between the films when the limited surfactant molecules in the films prefer to aggregate in bulk. As a result, C_8N/SDS exhibits the best oil cleaning and lowest foaming simultaneously at low X_{SDS} and just above the CMC. This study opens an efficient avenue to eliminate the contradiction between cleaning ability and foamability, thereby obtaining a high-efficiency and low-foam detergent.

Received 24th August 2023,
Accepted 27th September 2023

DOI: 10.1039/d3lf00145h

rsc.li/RSCApplInter

Introduction

Amphiphilicity of surfactants endows them with unique surface activity and self-assembly ability in aqueous solution, thus they are widely applied in many fields, such as consumer household cleaning products,[1–4] industrial cleaning,[5–7] food industry,[8,9] agriculture,[10–14] drug delivery,[15–18] *etc.* Particularly as detergents, the global surfactant market turnover reached USD 42.1 billion in 2020 according to the data from *Markets and Markets*™.[19] Moreover, the global cleaning products industry is projected to reach USD 61.6 billion by 2026.[20] Excessive consumption of surfactants causes environment chemical exposure and huge economic loss. With regard to this issue, many researchers have devoted their efforts in developing a wide range of novel surfactants by introducing more functional groups,[21–24] increasing the oligomerization degree,[25–28] and adjusting the length of the spacer or alkyl chain[29–31] so as to optimize the cleaning performance of surfactants and reduce their dosage by altering the static/dynamic surface tension,[32–35] adsorption kinetics,[36–39] aggregation ability,[40–42] *etc.* In parallel, mixing surfactants with additives (inorganic/organic salts, other surfactants, polymers, *etc.*) is also an effective way to adjust the physicochemical properties of surfactants at the surface/interface and in solution,[43–49] while a large number of commercial additives offer much more optionality, convenience and practicability. Hence, introducing appropriate additives into commonly used surfactants is undoubtedly an economic and convenient approach to obtain highly efficient surfactant systems and achieve sustainable development.

The generation of liquid foams is at the heart of numerous natural, technical, or scientific processes related to surfactants. In many cases, they have very useful properties for practical applications, such as cleaning, foam flotation, food processing and firefighting. However, foams are not always desirable. The unwanted foams can obstruct gas transport and render the process of interest ineffective with significant cost implications. Kister *et al.*[50,51] made a survey on causes of malfunctions in industry, and they found that the existence of foam in surfactant solutions in distillation processes was a major reason for 900 investigated cases of column malfunctions. The accumulation of impurities that stabilize the foam on the sea also produces foams and destroys the normal ecological

[a] *Beijing National Laboratory for Molecular Sciences and Institute of Chemistry, Chinese Academy of Sciences, Beijing 100190, P. R. China.*
E-mail: yxfan@iccas.ac.cn, yilinwang@iccas.ac.cn
[b] *Suzhou Institute for Advanced Research, University of Science and Technology of China, Suzhou, Jiangsu, 215123, P. R. China*
[c] *University of Science and Technology of China, Hefei, Anhui, 230026, P. R. China*
[d] *University of Chinese Academy of Sciences, Beijing 100049, P. R. China*
† Electronic supplementary information (ESI) available: Fig. S1–S7. See DOI: https://doi.org/10.1039/d3lf00145h

environment.[52–54] Coincidently, those aforementioned physicochemical properties facilitating the cleaning efficiency, such as low surface tension, strong aggregation ability and fast adsorption kinetics, often result in the strong foamability and foam stability in surfactant solution.[55–58] Therefore, the development of surfactant systems with high cleaning efficiency but adjustable foaming ability in different conditions encounters great technological hurdles although it is urgently desired in multiple fields.

The length and topological structure of alkyl chains play important roles in physicochemical properties of surfactants at surface/interface and in solution. Cyclic amines with bulky alkyl chains may form a larger hydrophobic domain in bulk but create looser arrangement at the air/water interface.[59,60] Their special structure makes it greatly possible for cyclic amine-containing systems to achieve high cleaning efficiency and low foam concurrently. Bearing in mind the structural advantages, we designed mixed systems composed of cyclic amines with various sizes of the cycloalkane ring (C_nN, n = 6, 8, 12) and widely used sodium dodecyl sulfate (SDS) at pH = 7.0. We found that the mixed solutions (C_nN/SDS) show lower CMC and surface tension and form various assemblies at different molar fractions of SDS (X_{SDS}) and total concentrations (C_T), driven by the electrostatic and hydrophobic interactions between SDS and cyclic amines. With the balance of the self-assembly of surfactants at the liquid film of foam and in bulk between the films, the oil cleaning efficiency of C_8N/SDS is much higher than that of the other two systems, whereas its foamability and foam stability are remarkably weakened. This work offers a feasible method for effectively removing oil with low foamability and foam stability at low surfactant concentrations, thereby potentially reducing surfactant usage and promoting sustainable development of environments.

Experimental section

Materials

Cyclohexylamine (C_6N, >99.5%) was purchased from Energy Chemical, cyclooctylamine (C_8N, >97%) was purchased from Acros Organics, cyclododecylamine (C_{12}N, >99%) was purchased from Leyan Chemical, sodium dodecyl sulfate (SDS, >99%) was purchased from Sigma-Aldrich, and hydrochloric acid (HCl, 36%) was purchased from Beijing Chemical Works. 20# machine oil was purchased from Kunlun Lubricant Company. Deionized water (18.2 MΩ cm) from Milli-Q equipment was used in all the experiments.

Surface tension measurement

The surface tension measurements of the C_nN/SDS (n = 6, 8, 12) mixed systems at different molar fractions of SDS (X_{SDS}) were carried out with a Wilhelmy plate method on the DCAT21 tensiometer (DataPhysics Co., Germany). The length and width of the plate were 19.90 and 0.20 mm, respectively. The standard error of surface tension is ~0.03 mN m^{-1}, and the test temperature was 25.00 ± 0.01 °C controlled by using a thermostat. Each measure was tested at least three times.

Turbidity measurement

The turbidity values of the C_nN/SDS (n = 6, 8, 12) mixtures at different C_T and X_{SDS} values, reported as 100 − % T, were measured at 450 nm using a Shimadzu UV-vis spectrophotometer (model UV-2800) with a water-circulating thermostat at 25.0 ± 0.01 °C. All the measured values were corrected by taking the turbidity of Milli-Q water as the controller.

Dynamic light scattering (DLS)

The size distribution of C_nN/SDS (n = 6, 8, 12) mixtures at C_T = 20 mM with X_{SDS} from 0 to 1.00 was measured using a Malvern ZetaSizer Nano ZS Instrument (ZEN3600, Malvern Instruments, Worcestershire, UK) at a scattering angle of 173° equipped with a 4 mW He–Ne laser (λ = 632.8 nm) and a thermosetting chamber at 25.0 ± 0.1 °C.

Cryogenic transmission electron microscopy (cryo-TEM)

5 μL C_6N/SDS solutions at X_{SDS} = 0.10, C_8N/SDS solutions at X_{SDS} = 0.20, 0.60 and C_{12}N/SDS solutions at X_{SDS} = 0.80 (C_T = 20 mM) were loaded onto a carbon-coated holey TEM grid. The excessive solution was sucked away by filter paper leaving a thin liquid film on the grid. After a few seconds, the grid was quickly vitrified by plunging into liquid ethane (cooled by liquid nitrogen) at −183 °C. The vitrified sample was transferred to a cryogenic sample holder and examined with a Themis 300 TEM (Thermo Fisher Scientific, America) at about −174 °C. The images were recorded on a Gatan charge-coupled device (CCD) camera in the minimal electron dose mode.

Interfacial tension measurement

The interfacial tension between surfactant mixtures and machine oil was measured by a TX500™ Spinning Drop Interface Tensiometer (Model TX500C). 1 mL C_nN/SDS (n = 6, 8, 12) mixtures at C_T = 5 mM with X_{SDS} from 0 to 1.00 were injected into a quartz glass tube as an external phase and 10 μL of machine oil was injected into liquid solution as an internal phase. Oil drop formations at different rotation rates were recorded by a CCD camera, and interfacial tension was calculated by measuring the length and width of the oil drop and using Vonnegut and Bashford–Adams fitting. All the measurements were tested at 25.0 ± 0.1 °C.

Contact angle measurement

C_nN/SDS (n = 6, 8, 12) mixture solutions at C_T = 5 mM with X_{SDS} from 0 to 1.00 were poured into a cuboid glass case. The stainless-steel plate was stuck to the bottom of a floating foam broad on the liquid solution. The machine oil droplet was squeezed out through a crooked needle and floated to the plate. The contact angle was recorded by a digital camera

and fitted by Image J software. Each measure was tested at least three times.

Cleaning measurement

Oil cleaning efficiency was determined by weighing the metage of the weight gap during cleaning progress. The weight of the stainless-steel plate was M_0. Each 50 μL of machine oil was daubed onto stainless-steel plates evenly. Stainless-steel plates with oil were weighed as M_1 and then soaked into 10 mL liquid solution at different ratios of SDS. After ultrasonic vibration in an ultrasonic cleaning tank with an ultrasonic power of 120 W at the temperature of 25 °C for 10 min, the oil on the stainless-steel plates was removed to different extent and weighed as M_2. All the measures were tested at least three times. The oil cleaning efficiency was calculated by using the following equation,

$$\text{Oil cleaning efficiency\%} = [(M_1 - M_2)/(M_1 - M_0)] \times 100$$

Foaming and defoaming measurement

The foaming and defoaming ability of various surfactant mixtures were tested by two methods. One is the air blowing method using a dynamic foam analyzer DFA 100 (KRÜSS, Germany). N_2 was continuously blown into 50 mL analyte liquor at the bottom of the container until the foam height did not increase, then the highest foam height was recorded as foaming ability. The state change of foams with time was recorded with a CCD camera, and bubble counts and half-time were recorded as defoaming ability. The other is the visual inspection method, *i.e.*, shaking 10 mL C_nN/SDS solutions of 5 mM at different X_{SDS} or fixed X_{SDS} = 0.10 with various C_T for 30 s. Following that, we recorded the change in foam height with aging and obtained the equilibrium foam height after resting for 2 h. The relative foam height is termed as the ratio of the measured foam height to the vial height.

Results and discussion

Self-assembly of C_nN/SDS mixtures at the air–water interface

The surface activity and the onset of micellization of SDS with a series of cyclic amines (C_nN, n = 6, 8, 12, Fig. 1A_1–A_3) were determined by surface tension measurements. Fig. 1B_1–B_3 show the surface tension curves for the C_nN/SDS mixtures as a function of the total concentration (C_T) at a fixed C_nN/SDS molar fraction ($X_{SDS} = C_{SDS}/(C_{SDS} + C_{C_nN})$, from 0.00 to 1.00). For comparison, the surface tension curves of pure SDS and C_nN aqueous solution are also included. Correspondingly, all the CMC and the surface tension at CMC (γ_{CMC}) of C_6N/SDS, C_8N/SDS and $C_{12}N$/SDS are summarized in Fig. 1C_1–C_3 to clearly show the influence of X_{SDS} on CMC and γ_{CMC}.

Obviously, the surface tension curves exhibit broadly similar profiles for all the C_nN/SDS mixtures regardless of the

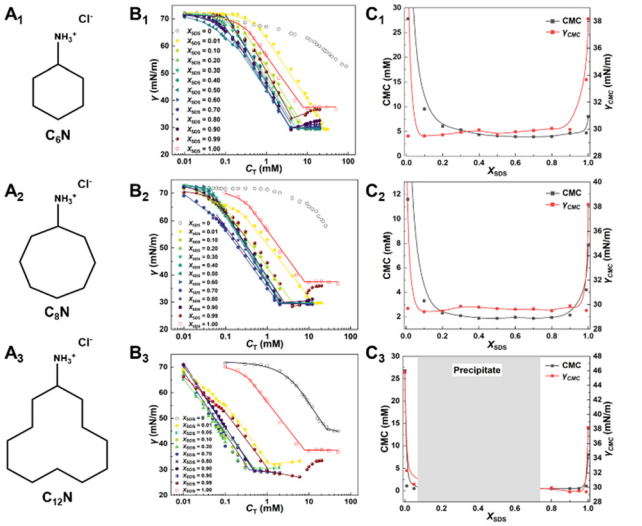

Fig. 1 Chemical structures and self-assembly behaviors of C_nN/SDS mixtures at the air/water interface. (A_1–A_3) Chemical structures of C_nN (n = 6, 8, 12). (B_1–B_3) Surface tension of (B_1) C_6N/SDS, (B_2) C_8N/SDS and (B_3) $C_{12}N$/SDS mixtures at 25.00 ± 0.01 °C. (C_1–C_3) The variation of CMC and γ_{CMC} values of (C_1) C_6N/SDS, (C_2) C_8N/SDS and (C_3) $C_{12}N$/SDS mixtures as a function of X_{SDS}.

sizes of the cycloalkane ring and the X_{SDS} values. The CMC value of SDS without C_nN derived from the breakpoint is 8.0 mM and the surface tension at CMC (γ_{CMC}) is 38 mN m^{-1}, which are consistent with previously reported values. For C_nN solution alone, the surface tension curves of C_6N and C_8N display no inflection point in the concentration range studied (<50 mM) and just show a slight decline to ~55 mN m^{-1}, whereas the CMC and γ_{CMC} values of $C_{12}N$ are 28 mM and 47 mN m^{-1}, indicating that the three cyclic amines possess a very weak surface activity. As expected, the molecular arrangement at the air/water interface of cyclic amines with a bulky alkyl chain is much looser than that of the alkyl amine with the same carbon number, *e.g.*, CMC and γ_{CMC} values of *N*-dodecylamine are 2.6 mM and 30 mN m^{-1} (Fig. S1†).

Upon mixing the two components, the CMC and γ_{CMC} values decrease significantly to lower than those of individual components, attributed to the strong electrostatic attraction between the cationic headgroup of protonated C_nN and the anionic sulfate of SDS and the hydrophobic interaction of the alkyl ring of amines with the alkyl chain of SDS. Even at X_{SDS} = 0.01, the CMC values have already reduced to 27.8, 11.6 and 1.1 mM for C_6N/SDS, C_8N/SDS and $C_{12}N$/SDS mixtures, respectively, whereas the γ_{CMC} values declined to ~30 mN m^{-1}, nearly 8.0 mN m^{-1} lower than that of the pure SDS solution. When X_{SDS} approaches 0.5 from 0 or 1.0, the CMC value is steadily decreased to the lowest one, *i.e.*, 4.0, 2.0 and 0.4 mM for C_6N/SDS, C_8N/SDS and $C_{12}N$/SDS, respectively, while the γ_{CMC} values are maintained at low values (~30 mN m^{-1}) and there is almost no further decrease with varying X_{SDS}. Thus, the variation of CMC and γ_{CMC} values displays similar trends to X_{SDS} changing from 0 to 1.0, *i.e.*, decreasing first and then reaching a plateau and increasing rapidly

again. It is worth noting that the surface tension curves of the mixed solutions at high X_{SDS} show an upward end with increasing C_T, which is attributed to the significant excess SDS, thus causing the increase in surface tension to reach the γ_{CMC} value of SDS itself. These results show that the binding affinity becomes stronger when the molar ratio of C_nN and SDS is close to 1 : 1, and the strong binding between the two components possibly induces the remarkable deformation or the transformation of the molecular configuration of C_nN,[60–62] thereby the molecular packing is significantly compacted at the air/water interface. However, the surface tension curves of the $C_{12}N$/SDS mixtures at $0.20 < X_{SDS} < 0.70$ are excluded because the precipitation takes place in such a wide range of X_{SDS}, which is different from the C_6N/SDS and C_8N/SDS mixtures with smaller cycloalkane rings. Despite these, we can still observe that the ability to reduce CMC is enhanced from C_6N/SDS to $C_{12}N$/SDS, demonstrating that the larger alkyl ring leads to the stronger hydrophobic interaction of the cyclic amines with SDS.

Aggregation behavior of C_nN/SDS mixtures in bulk

To further understand the impact of the cyclic amines with different sizes of the cycloalkane ring on the self-assembly of SDS in bulk, the aggregation behaviors of C_nN/SDS mixtures were studied by turbidity measurement (Fig. $2A_1$–A_3), dynamic light scattering (DLS, Fig. 2C) and cryogenic transmission electron microscopy (cryo-TEM, Fig. $2D_1$–D_3). The different aggregate structures were observed with changing X_{SDS} and C_T as depicted in phase diagrams (Fig. $2B_1$–B_3), which are derived from the turbidity curves of the C_nN/SDS aqueous solution as a function of C_T at various X_{SDS} values.

For C_6N/SDS, the turbidity value remains extremely low no matter which value X_{SDS} or C_T is. Taking the situation at C_T = 20 mM as a representative, the mean particle size remains below 20 nm. The broadly invariable turbidity and size as well as the lower CMC values (Fig. $1B_1$) demonstrate that the addition of C_6N promotes the micellization of SDS, but only induces the formation of small spherical or rodlike micelles, which is confirmed by the cryo-TEM micrographs of C_6N/SDS aggregates at X_{SDS} = 0.20 and C_T = 20 mM (Fig. S2†).

In contrast, the self-assembly behavior of SDS is significantly affected by C_8N and $C_{12}N$, and undergoes different processes at various X_{SDS} and C_T. For the C_8N/SDS mixture, there is almost no change in the turbidity with C_T as $X_{SDS} > 0.5$, indicating that the small fraction of C_8N has a strong ability to accelerate the micellization of SDS but not enough to affect the molecular packing and the aggregate structures. At $X_{SDS} > 0.5$, the turbidity values increase with increasing C_T, and the largest value appears at X_{SDS} = 0.40. Fixing C_T = 20 mM, a weakly bluish solution was observed, and the C_8N/SDS mixed solution forms vesicles of a few tens of nanometers at X_{SDS} = 0.20, while the solution becomes transparent and forms wormlike micelles with a few millimeters long at X_{SDS} = 0.60, as evidenced by the results of DLS (Fig. 2C) and cryo-TEM (Fig. $2D_1$ and D_2). Compared with the phase boundaries of C_8N/SDS and $C_{12}N$/SDS mixtures, they go through similar changing processes with increasing X_{SDS} at the same C_T, but the big differences take place at much lower X_{SDS} and C_T for the aggregate formation, the larger vesicles (>100 nm, Fig. $2D_3$) and the wider precipitate region over the C_T range in $C_{12}N$/SDS.

In summary, the addition of C_nN only promotes the micellization of SDS for C_6N, while leads to an aggregate transition from small micelles to vesicles and then to wormlike or spherical micelles at a fixed C_T for C_8N without precipitation and for $C_{12}N$ with a large range of precipitation. In all the three C_nN/SDS mixtures, the electrostatic interaction between the protonated amine and sulfate groups and the hydrophobic interaction among the alkyl chains of C_nN and SDS are the main driving forces for their self-assembly. However, taking a variety of conformations of cycloalkylamine in aqueous solution into account,[60–62] we speculate that both the size and conformation of the cycloalkane ring of C_nN may play a decisive role in the different aggregate formation and transition. Fig. 3 summarizes a simplified schematic diagram of aggregation behavior for the C_nN/SDS mixture in bulk with changing in X_{SDS} at a fixed C_T.

The C_6N molecule has the smallest cycloalkane ring. It is not long enough to enlarge the hydrophobic area in the aggregate relative to the SDS itself, thereby the C_6N/SDS

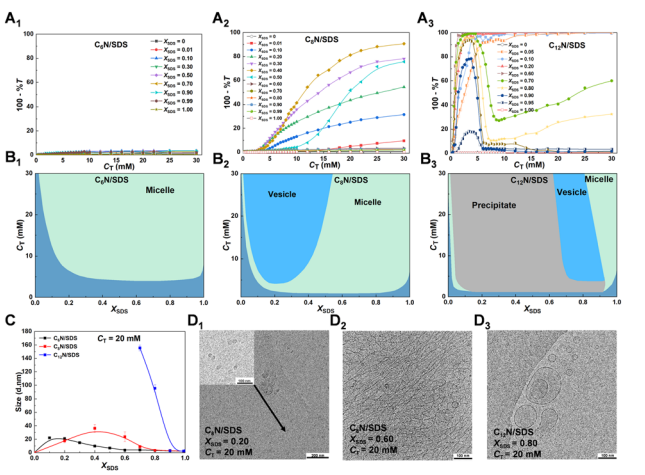

Fig. 2 Self-assembly of C_nN/SDS mixtures in bulk solution. (A_1–A_3) Turbidimetric curves of (A_1) C_6N/SDS, (A_2) C_8N/SDS and (A_3) $C_{12}N$/SDS at different X_{SDS} values measured by UV-vis spectroscopy. (B_1–B_3) Phase diagram of (B_1) C_6N/SDS, (B_2) C_8N/SDS and (B_3) $C_{12}N$/SDS mixtures. (C) The size variation of C_nN/SDS aggregates at C_T = 20 mM as a function of X_{SDS}. (D_1–D_3) Cryo-TEM images of the C_nN/SDS aggregates at C_T = 20 mM: (D_1) C_8N/SDS at X_{SDS} = 0.20, (D_2) C_8N/SDS at X_{SDS} = 0.60, and (D_3) $C_{12}N$/SDS at X_{SDS} = 0.80.

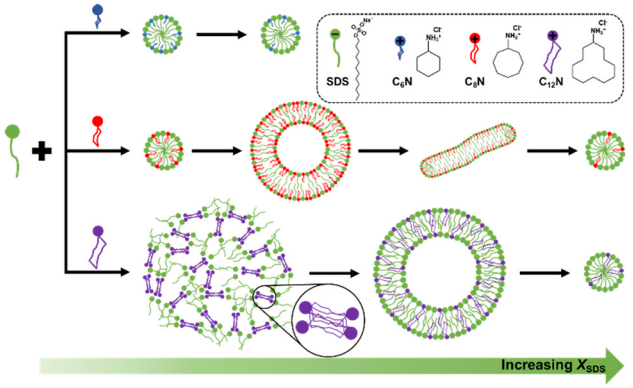

Fig. 3 The schematic illustrations of the variation of the aggregate morphologies in the C_nN/SDS mixtures with increasing X_{SDS}. In C_6N/SDS, only spherical micelles are formed regardless of C_T and X_{SDS}. In C_8N/SDS, the aggregates transit from spherical micelles to vesicles, wormlike micelles and then to spherical micelles again by increasing X_{SDS} from 0 to 1.00. In $C_{12}N$/SDS, the precipitate is formed rich in $C_{12}N$ because of the enhanced interaction between $C_{12}N$ and SDS due to the distinctive molecular conformation of $C_{12}N$. With increasing X_{SDS}, the precipitate is redissolved and transfers to vesicles and spherical micelles.

mixture only forms small micelles. In comparison, the C_8N molecule with a larger cycloalkane ring can produce stronger hydrophobic interaction with SDS and form a larger hydrophobic area. As such, the spontaneous curvature of the C_8N/SDS aggregates becomes slightly smaller, forming the wormlike micelles rich in SDS ($X_{SDS} > 0.5$) and vesicles rich in C_8N ($X_{SDS} < 0.5$). As for $C_{12}N$ with a much larger cycloalkane ring, it forms precipitate with SDS in a large range, which could be attributed to the remarkably enhanced hydrophobic interaction by the unique $C_{12}N$ ring. It was reported that the conformers of cyclooctane can be classified into three families, including boat–chair, chair–chair or crown, and boat–boat, while cyclododecane shows a square topology and has at least 100 possible conformations.[62] Thus, the large hydrocarbon ring is flexible enough to optimize the molecular conformation and nest together, in which case the ion pairs formed by $C_{12}N$ and SDS may be drawn closer with each other due to the tight entanglement between the $C_{12}N$ rings, thereby the precipitate with compact microstructure is formed, especially with the excessive $C_{12}N$. For the same reason, a small amount of $C_{12}N$ can lead to a significant change in the molecular packing of $C_{12}N$/SDS mixtures, thus the vesicles are formed at a large X_{SDS} (*e.g.*, $0.65 < X_{SDS} < 0.85$ at C_T = 20 mM). Hence, the cycloalkylamines with different sizes of rings lead to diverse aggregate structures, and the large chair conformation of $C_{12}N$ displays the most obvious effect on the association with SDS.

Oil-fouling removal efficiency of C_nN/SDS

Surfactants that form aggregates with a strengthened hydrophobic domain and show strong ability to enhance surface activity should be beneficial to strip and solubilize the oil from substrates, so we selected C_nN/SDS with C_T = 5 mM, which is higher than their CMC but as low as possible, to test the oil-fouling removal efficiency. Stainless-steel plates covered with machine oil-fouling were immersed into the C_nN/SDS solutions, and ultrasonically treated for 10 min, it was observed that the homogenous emulsion with machine oil was entrapped in the interior, or the machine oil was separated from the plate and suspended in the solution. After that, the stainless-steel plates were taken out from the solutions to evaluate the oil-fouling removal efficiency by inspection and weighting methods.

With the visual approach to observe the oil-fouling efficiency, we took the photos of residual oil on stainless-steel plates under ultraviolet light (UV) based on the blue light character of oil-foiling under UV light (Fig. 4A). For both the C_6N/SDS and C_8N/SDS mixtures, the area of blue light on plates becomes smaller first and then enlarges again with the increase of X_{SDS}, indicating that the optimum oil-fouling removal result appears around X_{SDS} = 0.5. The $C_{12}N$/SDS mixture follows the same changing pattern except for the precipitate region. In parallel, the quantitative evaluation by

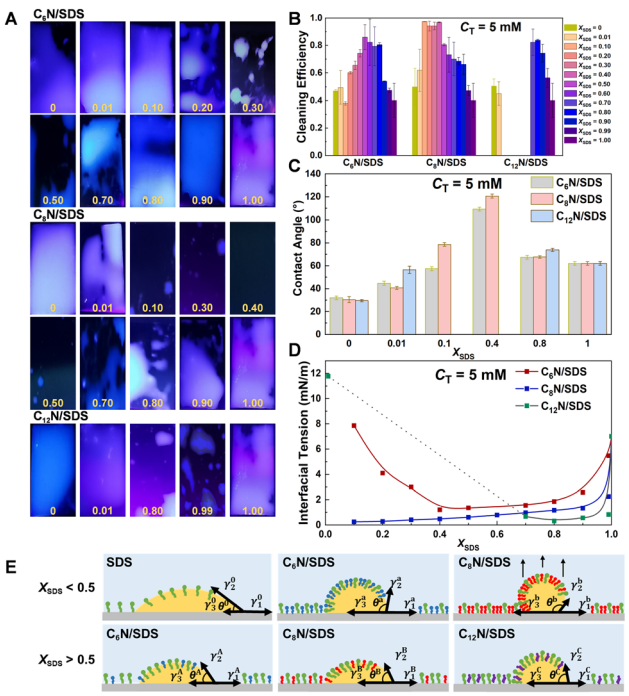

Fig. 4 Cleaning efficiency and mechanism of C_nN/SDS for removing machine oil contamination from stainless-steel plates. (A) Photos of stainless-steel plates contaminated with machine oil after ultrasonic cleaning by C_nN/SDS solutions at different X_{SDS} observed under the irradiation of UV light. The plates with machine oil contamination emit blue light under irradiation of UV light. (B) The oil-fouling cleaning efficiency of C_nN/SDS mixtures at different X_{SDS} by the weighting method. Oil cleaning efficiency% = $[(M_1 - M_2)/(M_1 - M_0)] \times 100$. (C) Solid/liquid contact angle of machine oil droplets on the stainless-steel plates under water with C_nN/SDS. (D) Oil/water interfacial tension values for machine oil in the C_nN/SDS solutions. In all the experiments, C_T was fixed at 5 mM. (E) The possible mechanism of oil-fouling cleaning efficiency for single SDS solution and C_nN/SDS (n = 6, 8, 12) mixtures.

the weighting method is summarized in Fig. 4B, also indicating that the X_{SDS} value for the highest oil-fouling removal efficiency is nearly 0.5. In addition, the C_8N/SDS system shows the wider X_{SDS} region ($0.1 < X_{SDS} < 0.5$) to reach high cleaning efficiency and the efficiency is better than that of C_6N/SDS. For $C_{12}N$/SDS, in the region without precipitation at larger X_{SDS}, it displays better cleaning performance than either C_6N/SDS or C_8N/SDS. That is, the C_nN/SDS mixture with a larger cycloalkylamine and stronger aggregation ability exhibits higher oil-fouling removal efficiency.

To further understand the role of cycloalkylamine size in the oil-fouling removal efficiency of C_nN/SDS, the cleaning process is investigated by oil–water interfacial tension and contact angles (θ) of oil on plate under solution (Fig. 4C and D). Normally, cleaning by surfactants is realized through the de-wetting mechanism,[63] for which the contact angles of oil drops on substrates under surfactant solutions are very large. Herein, the contact angles of machine oil drops on the plates in the C_nN/SDS solutions at the representative X_{SDS} show a similar changing trend with the oil-fouling cleaning performance, *i.e.*, good cleaning performance corresponds to a large contact angle. The oil-fouling tends to separate from the stainless-steel substrates at the medium X_{SDS} (Fig. 4C). Therefore, the de-wetting occurs around X_{SDS} = 0.5. Meanwhile, the interface tension between the oil and C_nN/SDS solutions becomes smaller than that of either C_nN or SDS, which is beneficial to the formation of O/W emulsion (Fig. 4D). And the O/W interfacial tension curves as a function of X_{SDS} display a concave edge, showing a contrary changing trend of cleaning efficiency curves. It means that both the de-wetting and emulsion are enhanced at the medium X_{SDS}, which facilitates the oil-fouling removal and impedes the separated oil to stick back on the substrates. Moreover, C_8N/SDS shows 0.5 mN m^{-1} lower interfacial tension than C_6N/SDS at $X_{SDS} < 0.50$, whereas $C_{12}N$/SDS shows the minimum interfacial tension at $X_{SDS} > 0.50$. As a result, the oil-fouling is readily dispersed into the C_nN/SDS solutions due to de-wetting and emulsion, and the highly efficient cleaning performance is obtained for C_8N/SDS at $X_{SDS} < 0.50$ and $C_{12}N$/SDS at $X_{SDS} > 0.50$.

Inspired by the Young's equation, we try to figure out the reasons for the various cleaning ability of C_nN/SDS solutions in the view of equilibrium of forces. Herein, the interfacial tensions of solid/water, oil/water and solid/oil are defined as γ_1, γ_2 and γ_3, respectively. The three parameters fit the equation, $\gamma_1 = \gamma_2 \cos\theta + \gamma_3$ (Fig. 4E). The contact angle of liquid on solid is proportional to the interfacial tension and energy, so according to the contact angles of C_nN/SDS (n = 6, 8, 12) solutions on the stainless-steel plates (Fig. S3†), the γ_1 values for pure SDS (γ_1^0), C_6N/SDS (γ_1^a) and C_8N/SDS (γ_1^b) at $X_{SDS} < 0.5$ are in order of $\gamma_1^0 > \gamma_1^a \approx \gamma_1^b$, while for C_6N/SDS (γ_1^A), C_8N/SDS (γ_1^B) and C_8N/SDS (γ_1^C) when $X_{SDS} > 0.5$, the order is $\gamma_1^A > \gamma_1^B > \gamma_1^C$. Meanwhile, $\gamma_2^0 > \gamma_2^a > \gamma_2^b$ at $X_{SDS} < 0.5$ and $\gamma_2^A > \gamma_2^B > \gamma_2^C$ at $X_{SDS} > 0.5$ are obtained from Fig. 4D. Combining with the order of contact angle of machine oil droplets on the plates in the C_nN/SDS solution (Fig. 4C), *i.e.*, $\theta^0 < \theta^a < \theta^b$ at $X_{SDS} < 0.5$ and $\theta^A < \theta^B < \theta^C$ at $X_{SDS} > 0.5$, we can observe that $\gamma_3^0 \leq \gamma_3^a < \gamma_3^b$ at $X_{SDS} < 0.5$ and $\gamma_3^A < \gamma_2^B < \gamma_2^C$ at $X_{SDS} > 0.5$. The results mean that the oil droplet has a stronger trend to retract inward and escape from the plate in C_8N/SDS at $X_{SDS} < 0.5$ or in $C_{12}N$/SDS at $X_{SDS} > 0.5$. All the experimental results and theoretical derivations provide insights into the cleaning efficiency of C_nN/SDS, from which the oil-foiling removal performance could be predicted by the oil/water interfacial tension and solid/liquid contact angle of oil droplets in surfactant solutions.

Foaming and defoaming test

For surfactant applications in cosmetics, detergents, food, *etc.*, strong foaming ability is normally needed. However, in industrial cleaning, petroleum refining and other large-scale applications, strong foamability and foam stability often lead to environmental hazards, wastewater treatment difficulty and economic loss. Therefore, surfactant systems with strong oil cleaning ability but weak foamability and foam stability are of importance in these fields.

Herein, to intuitively observe the foaming and defoaming ability of C_nN/SDS systems with great oil cleaning ability, we firstly shake 10 mL C_nN/SDS solutions of 5 mM for 30 s and record the change in foam height with aging (Fig. S4†). In parallel, we gain the variation of foam volume ($V_{foam\ max}$), foam state, foam height, and bubble counts with aging by using a dynamic foam analyzer (Fig. 5 and S5†). We compare foam state against aging for the C_6N/SDS and C_8N/SDS mixtures at fixed X_{SDS} = 0.10 mM and C_T = 5.0 mM with the visual inspection method (inset) and air blowing method using a dynamic foam analyzer (Fig. S6†), and apparently the visual and quantitative results are consistent with each other. C_nN (n = 6, 8, 12) alone almost has no ability to form liquid foams. With the addition of C_nN, the foamability characterized by the maximum foam volume ($V_{foam\ max}$, Fig. 5B) gradually becomes weaker with decreasing X_{SDS}, and the C_8N/SDS system displays the smallest foam volume when $X_{SDS} < 0.50$, especially at X_{SDS} = 0.10. Although the values of the maximum foam volume do not show significant differences, the differences in the foamability and foam stability are manifested in the changes of the bubble size, the foam heights and bubble count with time. Obviously, the low foamability of C_8N/SDS is further verified by the bigger bubbles formed at X_{SDS} = 0.10 and 30 s (Fig. 5A and S5†), following which the bubbles begin to break at 1500 s when the foams in pure SDS, C_6N/SDS (X_{SDS} = 0.10, 0.40, 0.50, 0.80), C_8N/SDS (X_{SDS} = 0.30, 0.40, 0.80) and $C_{12}N$/SDS ($C_{12}N$/SDS = 0.80) are still very stable. Correspondingly, the C_6N/SDS system shows the similar changing speed in foam height against aging compared with SDS, the $C_{12}N$/SDS system defoams also quite slowly, but the foam height of C_8N/SDS decreases 3–5 times faster than that of SDS itself (Fig. 5C). The bubble count of C_nN/SDS also confirms that the C_8N/SDS

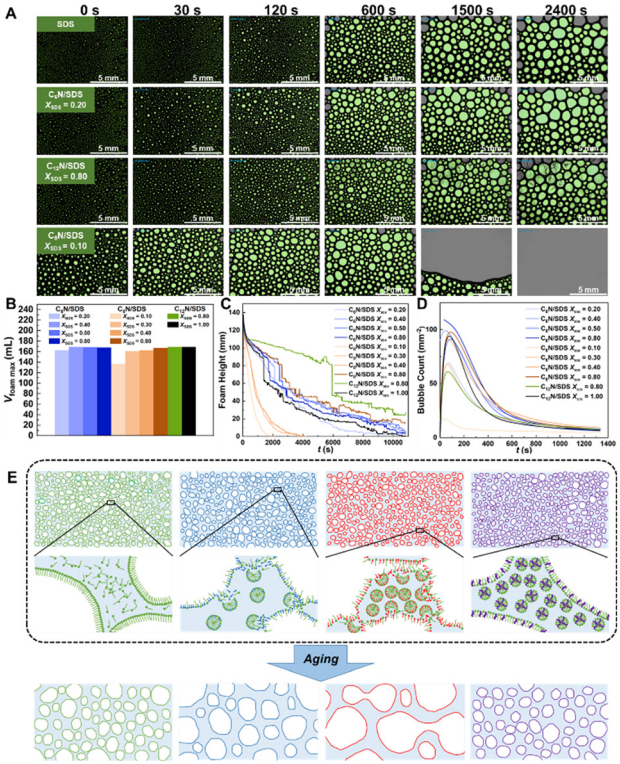

Fig. 5 Foamability and foam stability of C_nN/SDS (n = 6, 8, 12). (A) Images of foam state with aging recorded by a CCD camera for 5 mM SDS, 5 mM C_6N/SDS at X_{SDS} = 0.10, 5 mM C_8N/SDS at X_{SDS} = 0.10, and 5 mM C_{12}N/SDS at X_{SDS} = 0.80. The maximum foam volume after gas admission (B), the variation of foam height against aging (C) and the change of bubble count against aging (D) for C_nN/SDS mixtures at different X_{SDS}. (E) The possible mechanism of the decay process for foams in single SDS solution and C_nN/SDS (n = 6, 8, 12) mixtures.

system shows the fastest defoaming speed (Fig. 5D). All the above results demonstrate that the C_8N/SDS mixture at X_{SDS} < 0.50 can effectively reduce the foamability and enhance the defoam ability, perfectly corresponding to the condition for the high oil-fouling removal efficiency.

We speculate that there are two factors affecting the foam stability and defoaming ability of C_nN/SDS mixed systems: surface tension and dynamic molecular exchange between the bulk phase and air/water interface. The low surface tension manifests that the surfactant molecules prefer packing at the air/water interface, which contributes to the formation and stabilization of foams. However, all the C_nN/SDS systems reduce the surface tension of SDS from 38 mN m^{-1} to 30 mN m^{-1}, thus the foamability and foam stability should be improved in principle. Actually, only the C_{12}N/SDS system obeys this prediction, while the C_6N/SDS and C_8N/SDS systems exhibit similar or even weaker foamability and foaming stability than SDS. We turn back to analyze the C_T value we selected. In order to compare the foams, we selected the same C_T (5 mM), which is below the CMC of SDS (~8.0 mM) and C_6N/SDS (~6.0 mM), or much larger than that of C_{12}N/SDS (~0.40 mM), but only slightly higher than the CMC value of C_8N/SDS (~3.0 mM). In general, there are three different mechanisms governing the lifetime of foam: (i) foam drainage caused by gravity, (ii) coarsening caused by the transfer of gas between bubbles generated by the capillary pressure differences, and (iii) bubble coalescence caused by the rupture of liquid films between neighbouring bubbles.[64] For the present systems, it is proposed that the dynamic molecular exchange between the bulk phase and air/water interface can accelerate the enlargement and destruction of bubbles, which can perfectly explain the anomalous phenomenon in the foam (Fig. 5E). Given that the selected C_T is close to but below the CMC for SDS and C_6N/SDS, the surfactant molecules are enough to promote the adsorption saturation at the air/water interface but still have no ability to form micelles, in which case the molecules locating in the liquid film are relatively stable, resulting in the low defoaming ability. However, this C_T is much higher than the CMC of C_{12}N/SDS, which indicates that the absorption saturation has been completely reached at the air/water interface, and the number of molecules in the C_{12}N/SDS aqueous solution is large enough to form stable micelles, thereby the molecules at the air/water interface do not exhibit the tendency to enter the bulk solution, leading to the stronger foam stability. In comparison, the C_T is slightly higher than the CMC value of C_8N/SDS. In the foaming process of C_8N/SDS, more surfactant molecules join the air/water interface, while the real surfactant concentration in bulk is just high enough for micellization. The unstable bubble films promote the fusion of neighbour bubbles, and the surfactant molecules prefer to return to the micelles in bulk solution from the bubble films, *i.e.*, the air/water interface, leading to the enlargement and destruction of bubbles under this condition.

In brief, it is concluded that high oil cleaning efficiency and low foam stability of surfactant mixtures are achieved at an appropriate concentration, *i.e.*, above CMC, but not too large at a proper X_{SDS}. Inspired by the present results, we tested oil-fouling removal efficiency and foam height with the C_6N/SDS and C_8N/SDS mixtures after vortexing for 30 s and resting for 2 h at X_{SDS} = 0.10 and various C_T. For the given X_{SDS} at 0.10, we found that the cleaning efficiency becomes higher with the increase of C_T and is significantly enhanced especially above CMC. However, there is a

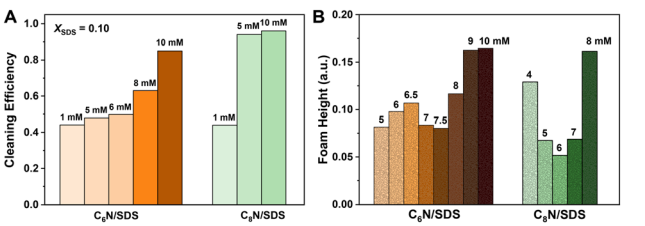

Fig. 6 The cleaning and foaming performance of C_nN/SDS (n = 6, 8) at X_{SDS} = 0.10 and different C_T. (A) The oil-fouling cleaning efficiency by the weighting method and (B) foam height after vortexing for 30 s and standing for 2 h for C_nN/SDS (n = 6, 8) at X_{SDS} = 0.10 and different C_T as marked in the plots.

minimum foam height just above CMC, after which the height becomes larger again (Fig. 6A and B, S7 and S8†). The CMC of C_6N/SDS is larger than that of C_8N/SDS, so the minimum appears at the larger concentration for C_6N/SDS, *i.e.*, at ~7.5 mM for C_6N/SDS and ~6.0 mM for C_8N/SDS. Combining with the continuous enhancement of cleaning efficiency and the minimum foam height above CMC, it can be speculated that selecting the concentration slightly above CMC at low X_{SDS} should be beneficial to obtain a high-efficiency and low-foam cleaning system. Therefore, the concentration of 5 mM used above meets the requirements for C_8N/SDS, resulting in good cleaning and deforming performance at $X_{SDS} < 0.50$. Due to the weaker self-assembly ability of C_6N/SDS at the air/water interface and in bulk, its performance in cleaning and defoaming efficiency cannot be better than that of C_8N/SDS.

Conclusions

In this work, we designed mixed surfactant systems composed of SDS and C_nN (n = 6, 8, 12) and studied their oil-fouling and foam removal ability. With addition of C_nN, the surface activity and aggregation ability of SDS are significantly enhanced, and the degree of enhancement is increased with the larger size of the cycloalkane ring because the hydrophobic interaction becomes stronger. As a result, only spherical micelles form in C_6N/SDS mixtures, while vesicles, spherical micelles and wormlike micelles form in the C_8N/SDS and C_{12}N/SDS mixtures. However, the flexible and adjustable cycloalkane ring of C_{12}N leads to the changeable conformation transformation and facilitates entanglement with each other tightly, thereby precipitation takes place in a large concentration range in C_{12}N/SDS. Except for the region of precipitate, the oil cleaning efficiency of C_nN/SDS shows a similar changing trend against X_{SDS} at a fixed C_T and the optimum condition mainly appears around X_{SDS} = 0.50. Meanwhile, the stronger aggregation ability induces the higher cleaning efficiency with increasing cycloalkane ring size and C_T. As a result, the best cleaning performance is achieved by C_8N/SDS in a broader X_{SDS} region, especially at low X_{SDS}. In parallel, the changing trend of foam stability is broadly consistent with cleaning efficiency against X_{SDS} for a given C_T, *i.e.*, the strong defoaming ability appears at $X_{SDS} < 0.5$, which is attributed to the low surface activity of C_nN. But it is totally different with changing C_T for a fixed X_{SDS}, *i.e.*, there is an obvious decline of foam ability slightly above CMC, which is driven by the migration of the limited molecules from the liquid film of foams to bulk between films for micellization. Due to the stronger self-assembly ability of C_8N/SDS than C_6N/SDS, the highly efficient foam removal is realized by C_8N/SDS at smaller C_T. It can be concluded that the highly efficient oil-fouling and foam removal can be achieved concurrently in a surfactant system mixing with an additive of relatively high solubilization and low surface activity like cyclic amines as we expected, which may form a larger hydrophobic domain in bulk through molecular conformation transition but create looser arrangement at the air/water interface because of bulky alkyl rings. This could also be realized in a single surfactant solution with such properties like star-shaped oligomeric surfactants. As such, the paradoxical self-assembly ability in bulk and at the air/water interface could induce a different changing tendency of cleaning and foaming performance against molar fraction or total concentration, providing a possible condition to achieve such a pair of contradictory properties. Thus, this work offers a simple approach obtain a high-efficiency and low-foam detergent with a low usage, meeting the requirements of some applications and supporting the sustainable development of the environment.

Author contributions

Z. Z., Y. F., and Y. W. designed the research. Y. F. and Y. W. supervised the experimental work. Z. Z. performed most of the experiments. J. Y. performed cryo-TEM experiments on the C_nN/SDS aggregates. T. W. and Z. Z. performed the experiments on cleaning measurements together. All authors discussed and contributed to the interpretation of the data. Z. Z. wrote the original manuscript, and Y. F. and Y. W. edited the manuscript.

Conflicts of interest

There are no conflicts to declare.

Acknowledgements

We are grateful for the financial support from the National Key R&D Program of China (2021YFA0716700), National Natural Science Foundation of China (21972149 and 21988102) and the Beijing National Laboratory for Molecular Sciences (BNLMS).

Notes and references

1 J. J. Scheibel, *J. Surfactants Deterg.*, 2004, **7**, 319–328.
2 J. J. Mueller and H. H. Wenk, *Chimia*, 2021, **75**, 752–756.
3 L. Golsteijn, R. Menkveld, H. King, C. Schneider, D. Schowanek and S. Nissen, *Environ. Sci. Eur.*, 2015, **27**, 1–12.
4 M. Bernat, C. Pey, M. J. Bermejo, B. Nogues, J. Vilaret and N. Siscart, *Riv. Ital. Sostanze Grasse*, 2007, **84**, 246–252.
5 H. Lee, G. Amy, J. W. Cho, Y. M. Yoon, S. H. Moon and I. S. Kim, *Water Res.*, 2001, **35**, 3301–3308.
6 J. A. Howarter, K. L. Genson and J. P. Youngblood, *ACS Appl. Mater. Interfaces*, 2011, **3**, 2022–2030.
7 T. Wang, Y. Si, S. Luo, Z. Dong and L. Jiang, *Mater. Horiz.*, 2019, **6**, 294–301.
8 J. Weiss, E. A. Decker, D. J. McClements, K. Kristbergsson, T. Helgason and T. Awad, *Food Biophys.*, 2008, **3**, 146–154.
9 I. Kralova and J. Sjoblom, *J. Dispersion Sci. Technol.*, 2009, **30**, 1363–1383.

10 J. Wang, Y. Fan, H. Wang, J. Yin, W. Tan, X. Li, Y. Shen and Y. L. Wang, *Chem. Eng. J.*, 2022, **430**, 132920.
11 D. P. Sachdev and S. S. Cameotra, *Appl. Microbiol. Biotechnol.*, 2013, **97**, 1005–1016.
12 P. Hu, J. An, M. M. Faulkner, H. Wu, Z. Li, X. Tian and J. P. Giraldo, *ACS Nano*, 2020, **14**, 7970–7986.
13 I. S. Curtis and H. G. Nam, *Transgenic Res.*, 2001, **10**, 363–371.
14 B. Liu, Y. Fan, H. Li, W. Zhao, S. Luo, H. Wang, B. Guan, Q. Li, J. Yue, Z. Dong, Y. L. Wang and L. Jiang, *Adv. Funct. Mater.*, 2021, **31**, 2006606.
15 Y. Luo, Z. Teng, Y. Li and Q. Wang, *Carbohydr. Polym.*, 2015, **122**, 221–229.
16 Y. Singh, J. G. Meher, K. Raval, F. A. Khan, M. Chaurasia, N. K. Jain and M. K. Chourasia, *J. Controlled Release*, 2017, **252**, 28–49.
17 C. H. Tsai, J. L. Vivero-Escoto, I. I. Slowing, I. Fang, B. G. Trewyn and V. S. Y. Lin, *Biomaterials*, 2011, **32**, 6234–6244.
18 R. Guagliardo, J. Perez-Gil, S. De Smedt and K. Raemdonck, *J. Controlled Release*, 2018, **291**, 116–126.
19 Surfactants market by type (anionic, non-ionic, cationic, and amphoteric), application (home care, personal care, industrial & institutional cleaning, textile, elastomers & plastics, agrochemicals, and food & beverage), region - global forecast to 2028, MARKETSANDMARKETS, 2023, **https://www.marketsandmarkets.com/Market-Reports/biosurfactants-market-493.html**.
20 Industrial cleaning chemicals market by ingredient type (surfactants, solvents, chelating agents), product (gerernal & medical cleaning), application (manufacturing & commerical offices, healthcare, retail & food service), and region - global forecast to 2028, MARKETSANDMARKETS, 2023, **https://www.marketsandmarkets.com/Market-Reports/industrial-institutional-cleaning-chemicals-market-52902227.html**.
21 T. Wang, Y. Han, S. Dai, J. Wang, B. Liu, M. Cao, B. Guan and Y. L. Wang, *Nano Res.*, 2023, **16**, 2551–2562.
22 B. O. Okesola and A. Mata, *Chem. Soc. Rev.*, 2018, **47**, 3721–3736.
23 G. Ren, M. Wang, L. Wang, Z. Wang, Q. Chen, Z. Xu and D. Sun, *Langmuir*, 2018, **34**, 5798–5806.
24 Q. Zeng, Q. Li, Y. Huang, Y. Lv, X. Liao and Q. Yang, *J. Macromol. Sci., Part B: Phys.*, 2015, **54**, 329–347.
25 Y. Fan, Y. Hou, J. Xiang, D. Yu, C. Wu, M. Tian, Y. Han and Y. L. Wang, *Langmuir*, 2011, **27**, 10570–10579.
26 D. Yu, Y. Wang, J. Zhang, M. Tian, Y. Han and Y. L. Wang, *J. Colloid Interface Sci.*, 2012, **381**, 83–88.
27 L. Zhu, Y. Tang and Y. L. Wang, *J. Surfactants Deterg.*, 2016, **19**, 237–247.
28 R. Zana, *Adv. Colloid Interface Sci.*, 2002, **97**, 205–253.
29 D. Shao, G. Liu, H. Chen, C. Xu and J. Du, *J. Surfactants Deterg.*, 2021, **24**, 357–364.
30 M. Wang, Y. Wang, D. Yu, Y. Han and Y. L. Wang, *Colloid Polym. Sci.*, 2013, **291**, 1613–1621.
31 R. Zana, *J. Colloid Interface Sci.*, 2002, **248**, 203–220.
32 S. A. Onaizi, *Eur. Biophys. J.*, 2018, **47**, 631–640.
33 F. G. Valeeva, E. A. Vasilieva, G. A. Gaynanova, R. R. Kashapov, S. V. Zakharov, D. A. Kuryashov, S. S. Lukashenko, N. Y. Bashkirtseva and L. Y. Zakharova, *J. Mol. Liq.*, 2015, **203**, 104–110.
34 A. Bera, K. Ojha and A. Mandal, *J. Surfactants Deterg.*, 2013, **16**, 621–630.
35 J. Eastoe and J. S. Dalton, *Adv. Colloid Interface Sci.*, 2000, **85**, 103–144.
36 N. Genc, E. Durna and O. Kilicoglu, *J. Water Chem. Technol.*, 2019, **41**, 236–241.
37 B. Riechers, F. Maes, E. Akoury, B. Semin, P. Gruner and J. C. Baret, *Proc. Natl. Acad. Sci. U. S. A.*, 2016, **113**, 11465–11470.
38 A. Bera, T. Kumar, K. Ojha and A. Mandal, *Appl. Surf. Sci.*, 2013, **284**, 87–99.
39 S. Paria and K. C. Khilar, *Adv. Colloid Interface Sci.*, 2004, **110**, 75–95.
40 D. Yu, Q. Zhang, C. Wu, Y. Wang, L. Peng, D. Zhang, Z. Li and Y. L. Wang, *J. Phys. Chem. B*, 2010, **114**, 8934–8940.
41 M. Deng, M. Cao and Y. L. Wang, *J. Phys. Chem. B*, 2009, **113**, 9436–9440.
42 M. L. Free, *Corros. Sci.*, 2002, **44**, 2865–2870.
43 Y. Chen, F. Qiao, Y. Fan, Y. Han and Y. L. Wang, *Langmuir*, 2017, **33**, 2760–2769.
44 S. Luo, Y. Wang, M. Wang and Y. L. Wang, *J. Surfactants Deterg.*, 2018, **21**, 899–908.
45 Z. Chen, J. Penfold, P. Li, J. Doutch, Y. Fan and Y. L. Wang, *Soft Matter*, 2017, **13**, 8980–8989.
46 C. Zhou, D. Wang, M. Cao, Y. Chen, Z. Liu, C. Wu, H. Xu, S. Wang and Y. L. Wang, *ACS Appl. Mater. Interfaces*, 2016, **8**, 30811–30823.
47 J. Larsson, A. E. Leung, C. Lang, B. Wu, M. Wahlgren, T. Nylander, S. Ulvenlund and A. Sanchez-Fernandez, *J. Colloid Interface Sci.*, 2021, **585**, 178–183.
48 Q. Cui, J. Z. Liu, L. Yu, M. Z. Gao, L. T. Wang, W. Wang, X. H. Zhao, Y. J. Fu and J. C. Jiang, *J. Cleaner Prod.*, 2020, **274**, 122652.
49 A. Bhadani, A. Kafle, T. Ogura, M. Akamatsu, K. Sakai, H. Sakai and M. Abe, *Curr. Opin. Colloid Interface Sci.*, 2020, **45**, 124–135.
50 H. Z. Kister, *Chem. Eng. Res. Des.*, 1997, **75**, 563–589.
51 H. Z. Kister, *Chem. Eng. Res. Des.*, 2003, **81**, 5–26.
52 W. Dou, Z. Zhang, W. Huang, X. Wang, R. Zhang, Y. Wu, A. Sun, X. Shi and J. Chen, *Chemosphere*, 2022, **303**, 135032.
53 L. Polasek, J. Bering, H. Kim, P. Neitlich, B. Pister, M. Terwilliger, K. Nicolato, C. Turner and T. Jones, *Mar. Pollut. Bull.*, 2017, **117**, 371–379.
54 K. Schilling and M. Zessner, *Water Res.*, 2011, **45**, 4355–4366.
55 D. Shao, G. Liu, H. Chen, C. Xu and J. Du, *J. Surfactants Deterg.*, 2021, **24**, 357–364.
56 P. Pal, I. Shittu, J. Oladunni and F. Banat, *J. Nat. Gas Sci. Eng.*, 2020, **81**, 103478.
57 Y. Sheng, X. Wu, S. Lu and C. Li, *J. Surfactants Deterg.*, 2016, **19**, 823–831.
58 Q. Liu, S. Zhang, D. Sun and J. Xu, *Colloids Surf., A*, 2010, **355**, 151–157.
59 P. W. Pakes, T. C. Rounds and H. L. Strauss, *J. Phys. Chem.*, 1981, **85**, 2469–2475.

60 I. Kolossvary and W. C. Guida, *J. Am. Chem. Soc.*, 1993, **115**, 2107–2119.
61 Y. Wang, P. Kirsch, T. Lebl, A. M. Z. Slawin and D. O'Hagan, *Beilstein J. Org. Chem.*, 2012, **8**, 1271–1278.
62 E. J. Saavedra, S. A. Andujar, F. D. Suvire, M. A. Zamora, M. L. Freile and R. D. Enriz, *Int. J. Quantum Chem.*, 2012, **112**, 2382–2391.
63 B. Liu, T. Li, W. Y. Wang, L. M. C. Sagis, Q. P. Yuan, X. G. Lei, M. A. C. Stuart, D. Li, C. Bao and J. Bai, *et al.*, *Nat. Sustain.*, 2020, **3**, 448–458.
64 I. Cantat, S. Cohen-Addad, F. Elias, F. Graner, R. Hohler, O. Pitois, F. Rouyer and A. Saint-Jalmes, *Foams: structure and dynamics*, Croydon: CPI Group (U.K.) Ltd, 2013.